



# A simple solution method to prepare VO<sub>2</sub>:Co<sup>2+</sup> precursors for thin film deposition by solution-processing method

Un método simple de solución para preparar películas delgadas de VO<sub>2</sub>:Co<sup>2+</sup> para la deposición mediante el método de procesamiento en solución

F. Hernandez-Guzman<sup>a</sup>, G. Suarez-Campos<sup>a,b,\*</sup>, D. Cabrera-German<sup>a</sup>, M.A. Millan-Franco<sup>c</sup>, H. Hu<sup>c</sup>, M.A. Quevedo-Lopez

<sup>a,d</sup>, M. Sotelo-Lerma<sup>a\*</sup>

<sup>a</sup> Department of Research in Polymers and Materials, University of Sonora, Hermosillo, Sonora, Mexico.

<sup>b</sup> Department of Chemical Engineering and Metallurgy, University of Sonora, Hermosillo, Sonora, Mexico.

<sup>c</sup> Institute of Renewable Energies, National Autonomous University of Mexico, Temixco, Morelos, Mexico

<sup>d</sup> Materials Science and Engineering Department, University of Texas at Dallas, Richardson, United States.

## ABSTRACT

Solution-processing is a low-cost solution method to prepare a variety of organic or inorganic thin films. For metal oxide compounds, a solution-processing solution of an organometallic compound is frequently used as a precursor to be spin coated, followed by a thermal annealing to form metal oxide. In this work, vanadium oxide powders are obtained from a simple acid-base reaction, and then they are dispersed in isopropyl alcohol to form a solution for spin-coating. Different amount of cobalt salt are also added together with VO<sub>x</sub> into isopropyl alcohol to form VO<sub>x</sub>:Co<sup>2+</sup> solutions. After thermal annealing at 200 °C, continuous transparent thin films are obtained. Optical, structural, morphological and chemical binding energies of those films are analyzed. It is found that amorphous VO<sub>2</sub>:Co<sup>2+</sup> compound is formed in those films with V:Co atomic ratios between 6.6:1 and 1.6:1. Optical absorption onsets of those films are around 2.3 eV. An interesting interconnected porous morphology is observed when the atomic ratio of V:Co is around 4.9:1. It is concluded that porous amorphous cobalt doped vanadium oxide thin films can be obtained from a spin-coating process at low annealing temperature from a simple solution without any complex agent.

**Keywords:** cobalt doped vanadium oxide, spin-coated thin films, porous morphology, solution processing without ligands.

## RESUMEN

El procesamiento de soluciones es un método de bajo costo para preparar una variedad de películas delgadas orgánicas o inorgánicas. Para compuestos de óxidos metálicos, un procesamiento de solución de un compuesto organometálico se usa con frecuencia como solución precursora para ser recubierta por rotación, seguida de un tratamiento térmico para formar el óxido metálico. En este trabajo se obtienen polvos de óxido de vanadio a partir de una simple reacción ácido-base, y luego se dispersan en alcohol isopropílico para formar una solución para spin-coating. También se agregan diferentes cantidades de sal de cobalto junto con VO<sub>x</sub> en alcohol isopropílico para formar soluciones de VO<sub>x</sub>:Co<sup>2+</sup>. Después

del tratamiento térmico a 200 °C, se obtienen películas delgadas transparentes. Se analizan las propiedades ópticas, estructurales, morfológicas y químicas. Se encontró que el compuesto VO<sub>2</sub>:Co<sup>2+</sup> es amorfo y se obtiene con una relación atómica V:Co variada de 6.6:1-1.6:1. El material presenta una absorción óptica alrededor de 2.3 eV. Se observa una interesante morfología porosa interconectada cuando la relación atómica de V:Co es ~4.9:1. Se concluye que se pueden obtener películas delgadas amorfas porosas de VO<sub>2</sub>:Co<sup>2+</sup> a partir del spin-coating a una baja temperatura de tratamiento utilizando una solución simple sin agente complejante.

**Palabras clave:** óxido de vanadio dopado con cobalto, películas delgadas mediante recubrimiento centrifugo, morfología porosa, procesamiento de la solución sin complejantes.

## INTRODUCTION

Vanadium oxides (VO<sub>x</sub>) and VO<sub>x</sub> doped with different metal oxides are interesting semiconductor materials because of their abundance in the Earth's crust, as well as its multi-oxidation states and various crystalline structures (Silversmit *et al.*, 2004, 2006). As a semiconductor material, VO<sub>x</sub> shows a band gap ~2.6-3.5 eV that makes it a good semiconductor material for diverse electronic application. In the literature, VO<sub>x</sub> thin films have been deposited with different methods for diverse potential applications employing techniques such as: magnetron sputtering and spin-coating for thermochromic applications (Ho *et al.*, 2019; Zhan *et al.*, 2020; Yuan *et al.*, 2021); pulsed laser deposition for cathodes in Lithium and sodium-ion batteries (Petnikota *et al.*, 2018); sprayed solution for NO<sub>2</sub> gas sensing (Khatibani, Abbasi and Rozati, 2016; Mane and Moholkar, 2017); solution-processing method for smart windows applications (Peng *et al.*, 2018; Wang *et al.*, 2020; Shen *et al.*, 2021).

On the other hand, modifications of optical or structural properties of semiconductor thin films are necessary to improve application of these materials. Which by adding a different type of metal ions into a VO<sub>x</sub> host matrix, known as a doping process, is one of the most effective ways to modify vanadium oxide structure, leading to different electrochemi-

\*Author for correspondence: G Suarez Campos, M Sotelo-Lerma  
e-mail: guillermo.suarez@unison.mx, merida.sotelo@unison.mx

Received: November 3, 2022

Accepted: March 6, 2023

cal, catalytic, and magnetic properties (Lu *et al.*, 2019; Sharma *et al.*, 2021; Geng *et al.*, 2022). Metal doped vanadium oxide thin films have been obtained with different deposition techniques: Y-doped VO<sub>x</sub> thin films by DC reactive magnetron sputtering for electrical modulation applications (Zhou *et al.*, 2020); Cs-doped VO<sub>x</sub> thin films deposited by spun-cast as a hole extraction layer in perovskite solar cells (Yao *et al.*, 2018); Fe-doped VO<sub>x</sub> by sol-gel spin-coated for electrochromic device applications (Bae, Koo and Ahn, 2019); In-doped VO<sub>x</sub> thin films obtained by spray pyrolysis coating system for optical transparency modulation (Tabatabai Yazdi, Pilevar Shahri and Shafei, 2021); Co-doped VO<sub>x</sub> thin films by microwave irradiation process for battery-type supercapacitor applications (Liu *et al.*, 2020), among others (Ji *et al.*, 2018; Li *et al.*, 2019; Xu *et al.*, 2019).

Solution-processing spin-coating is an economical method to obtain homogeneous pure or doped VO<sub>x</sub> thin films. Compared to other chemical solution deposition methods, this method has the advantage that it enables the deposition of metal oxide thin films without seed layer on substrates such as glass, fluorine doped tin oxide (FTO), indium doped tin oxide (ITO) or coated polyethylene (PET) for transparent or flexible electronics applications (Hajzeri *et al.*, 2012). In particular, metal ion doping in VO<sub>x</sub> thin films could be an in-situ process in a spin-coating method by adding the metal source into the vanadium precursor solution. However, expensive organometallic compounds are usually employed to prepare metal precursor solutions. In this work, we propose a simple method to prepare vanadium oxide and cobalt doped vanadium oxide solutions, without the use of organometallic compound or any complex agent that would result in a slow metal cation release, and an increased time and temperature deposition. Chemical photoelectron analysis of vanadium oxide samples, with or without cobalt doping, confirms the formation of a vanadium oxide VO<sub>2</sub> compound in the film samples. Cobalt oxide CoO also prevails in VO<sub>2</sub>:Co<sup>2+</sup> samples, with some neighboring atoms arranged in a short-range order. Porous surface of VO<sub>2</sub>:Co<sup>2+</sup> thin films can be obtained, giving an optical absorption onset at 2.3 eV.

## EXPERIMENTAL PROCEDURE

### Synthesis of VO<sub>x</sub> powders and solution

Precursor solutions for VO<sub>x</sub> powders were prepared by using 0.1 M solution of vanadium (IV) oxide sulfate hydrate (VOSO<sub>4</sub>·xH<sub>2</sub>O) and 1 M solution of sodium hydroxide (NaOH), as previously suggested [25]. These two precursor solutions were mixed, resulting in a blue color solution with a pH ~2 tested with a MColorHast™. After that, the blue solution was heated at 80 °C for 3 h to obtain VO<sub>x</sub> precipitates. These precipitates were dispersed in methanol to dissolve possible impurities and then centrifuged. After centrifugation, VO<sub>x</sub> precipitates were dried at 80 °C for 2 h to obtain VO<sub>x</sub> powders.

To prepare a VO<sub>x</sub> sol-gel solution, VO<sub>x</sub> powders were dispersed in isopropyl alcohol under ultrasonic vibration at room temperature for 10 min. Then, the mixture solution was filtered with a cotton filter to remove the undispersed precipitates

and obtain a transparent solution for thin film deposition by spin-coating. Pure VO<sub>x</sub> films were called samples S<sub>1</sub>.

### Preparation of VO<sub>x</sub>:Co solutions

To obtain cobalt doped VO<sub>x</sub> precursor solutions, dried VO<sub>x</sub> powders and CoCl<sub>2</sub>·6H<sub>2</sub>O salt were dispersed/dissolved in isopropyl alcohol. Then, the solutions were subjected to ultrasonic vibration at room temperature for 10 min. Finally, the solutions were filtered with a cotton filter to remove the undispersed precipitates and obtain transparent VO<sub>x</sub>:Co solutions for thin film deposition by spin-coating. Four VO<sub>x</sub>:Co solutions were prepared with VO<sub>x</sub>/CoCl<sub>2</sub>·6H<sub>2</sub>O weight ratios of 0.7/0.3, 0.5/0.5, 0.3/0.7 and 0.1/0.9, called samples S<sub>2</sub>, S<sub>3</sub>, S<sub>4</sub> and S<sub>5</sub>, respectively.

### VO<sub>x</sub> and VO<sub>x</sub>:Co thin film deposition

The five precursor solutions, VO<sub>x</sub> and VO<sub>x</sub>/Co, were used to form thin films by spin-coating. Microscope glass slides from VE-P10 Velab™, to be used as substrates for vanadium oxide solutions, were washed with Alconox® detergent, rinsed with distilled water and air-dried. The clean substrates were placed in the Chemat Technology Spin-Coated KW-4A, 50 µL of the VO<sub>x</sub> or VO<sub>x</sub>:Co solutions were deposited at 2500 rpm for 2 min on the glass substrates. The obtained coatings were thermally annealed in air at 200 °C for 1 h and became solid thin films.

### Thin films characterizations

X-ray photoelectron spectroscopy (XPS) was used to assess the chemical composition of the films. The tool employed was PHI 5000 Versa Probe II, with a monochromatic Al Kα (1486.6 eV) X-ray source with a 0.1 eV step size and a constant pass energy of 23.50 eV. The scale of binding energies was corrected by calibrating the main C 1s peak at a binding energy of 284.8 eV. Atomic compositions of VO<sub>x</sub>/Co films were estimated from the XPS results. Crystalline structures of VO<sub>x</sub>/Co films were probed with X-ray diffraction (XRD) employing a Rigaku DMAX-2200 diffractometer equipped with a Cu Kα (λ = 1.54 Å) X-ray source. A Jeol JSM-7800F field emission scanning electron microscope (FE-SEM) was used to evaluate the surface morphology of the films. The surface morphology of each film sample was analyzed by atomic force microscopy (AFM) with a Veeco Dimension Icon, Bruker instrument. Optical transmittance spectra of VO<sub>x</sub>/Co films were measured with a Perkin Elmer Lambda 20 UV-visible spectrometer. Thicknesses of VO<sub>x</sub> and VO<sub>x</sub>:Co thin films were measured with an Ambios Technology XP 200 profilometer.

## RESULTS AND DISCUSSION

### Profilometry and main characteristics

The first assessment of the possible formation of continuous VO<sub>x</sub> and VO<sub>x</sub>:Co thin films from the above mentioned precursor solutions is film thickness measurement by profilometry. Table 1 lists the five types of VO<sub>x</sub>:Co thin films with their respective thickness. In the Alpha-Step profiles of all film samples, large grains of 100 to 400 nm of height were observed

ved and were embedded in continuous solid coatings with thickness from 133 to 246 nm.

**Table 1.** Thickness, band gap and V:Co atomic ratio of  $\text{VO}_x$ :Co film samples.  
**Tabla 1.** Grosor, brecha de banda y proporción atómica V:Co de muestras  $\text{VO}_x$ :Co.

Sample name	Weight ratio ( $\text{VOSO}_4 \cdot x\text{H}_2\text{O} / \text{CoCl}_2 \cdot 6\text{H}_2\text{O}$ )	Thickness (nm)	Atomic ratio of V:Co
$S_1$	1/0	$152 \pm 44$	1:0
$S_2$	0.7/0.3	$133 \pm 39$	6.6:1
$S_3$	0.5/0.5	$123 \pm 19$	4.9:1
$S_4$	0.3/0.7	$133 \pm 26$	2.9:1
$S_5$	0.1/0.9	$246 \pm 11$	1.6:1

### Optical properties

Optical transmittance spectra of  $\text{VO}_x$ :Co thin films can be appreciated in Figure 1a with transmittance percentage of 65 - 75 % in the 800 -1350 nm wavelength ( $\lambda$ ) range. The main influence of  $\text{Co}^{2+}$  inclusion is observed in UV-A to blue region, at 325 - 500 nm, as reported elsewhere (Hajzeri *et al.*, 2012; Martínez-Gil *et al.*, 2020). Furthermore, samples with larger  $\text{Co}^{2+}$  concentration, such as  $S_4$  and  $S_5$ , show lower transmittance at the visible region (400 - 700 nm). Optical absorption coefficient spectrum of each film sample,  $\alpha(\lambda)$  (Figure 1b), is calculated from the simplified Beer-Lambert equation:  $\alpha = -\frac{1}{d} \ln(T)$ , where  $d$  is film thickness and  $T(\lambda)$  the transmittance spectrum. The optical absorption onset (or band gap  $E_g$ ) value is estimated by intersection of two straight fitting lines. The  $E_g$  values of pure vanadium oxide and vanadium with different amounts of  $\text{Co}^{2+}$ , are around 2.3 eV, which is very close to that previously reported for  $\text{V}_2\text{O}_5$  [27]. It is also observed that the absorption coefficients of all the cobalt doped vanadium oxide thin films (from  $S_2$  to  $S_5$ ) are higher compared to the pure vanadium oxide sample ( $S_1$ ), keeping the same forms of the spectra. Higher absorption region ( $> 3.8$  eV) in these samples should be related to the glass substrate absorption.

### X-ray diffraction

X-ray diffraction pattern of  $\text{VO}_x$  film sample ( $S_1$ ) is presented in Figure 2, which appears to correspond to an amorphous material due to the broad signal around  $22^\circ$ , plus a monoclinic phase of  $\text{HNaV}_6\text{O}_{16} \cdot 4\text{H}_2\text{O}$  with the plane orientation (100) at around  $2\theta \sim 8^\circ$  (JCPDS# 49-0996 (Channu *et al.*, 2011)). This crystalline compound could be a residual from  $\text{VOSO}_4 \cdot x\text{H}_2\text{O} + \text{NaOH}$ , reaction and was not be eliminated during the  $200^\circ\text{C}$  annealing or the thin film processing. Interestingly, after  $\text{Co}^{2+}$  addition, the reflection peak around  $2\theta \sim 8^\circ$  gradually reduces. The higher the concentration of  $\text{Co}^{2+}$ , the smaller the intensity of that peak, until its complete elimination in the sample with the highest concentration of  $\text{Co}^{2+}$  (sample,  $S_5$ ).  $S_5$  shows the diffraction pattern typical of an amorphous film, hence it is a predominantly amorphous material. Since no diffraction peaks of  $\text{CoO}_x$  or  $\text{VCoO}_x$  compounds appear in the five  $\text{VO}_x$ : $\text{Co}^{2+}$  samples, it seems that low temperature annealing leads to amorphous materials, as indicated in (Hu *et al.*, 2017; Martínez-Gil *et al.*, 2020).

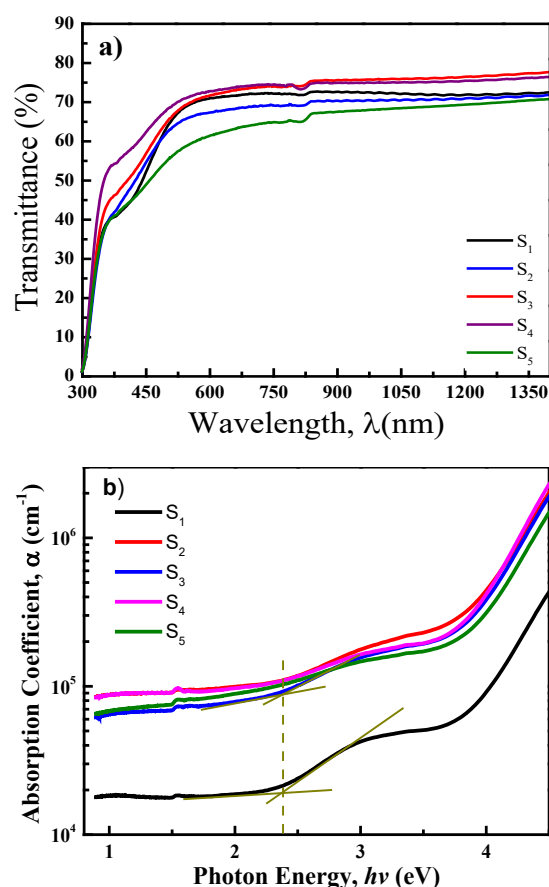


**Figure 1.** (a) Transmittance and (b) optical absorption coefficient spectra of vanadium oxide ( $S_1$ ) and cobalt doped vanadium oxide ( $S_2$  to  $S_5$ ) thin films.

**Figura 1.** Espectros de transmitancia (a) y coeficiente de absorción óptica (b) para películas delgadas de óxido de vanadio ( $S_1$ ) y óxido de vanadio dopado ( $S_2$  to  $S_5$ ).

### Thin films surface morphology

Figure 3 shows AFM three dimensional surface topography images in scales of  $2\text{ m} \times 2\text{ }\mu\text{m}$  of (a)  $S_1$ , (b)  $S_2$ , (c)  $S_3$ , (d)  $S_4$  and (e)  $S_5$   $\text{VO}_x$ : $\text{Co}^{2+}$  film samples. The root-mean-square roughness of the same samples is plotted in Figure 3f. The surface topography of pure  $\text{VO}_x$  film ( $S_1$ ) presents lumps and the lowest roughness. As the cobalt ions are incorporated into  $\text{VO}_x$  host, variations in shape and roughness are observed in AFM images. Notable changes are observed in samples  $S_3$  and  $S_4$  that exhibit a ring like morphology and increased roughness (8 - 9 nm) in comparison with  $S_1$  and  $S_2$  (4 - 5 nm) samples. sample  $S_5$  that contains the highest cobalt concentration loses the ring pattern in its surface morphology and shows the highest roughness ( $\sim 23$  nm) among the five samples. Similar results are reported elsewhere, suggesting that the inclusion of  $\text{Co}^{2+}$  in  $\text{VO}_x$  host by solution methods modifies the superficial morphology of cobalt doped vanadium oxide thin films (Fuentes-Ríos *et al.*, 2021). Such porous morphology encourages potential use of  $\text{VO}_x$ : $\text{Co}^{2+}$  thin films as a cathode material for lithium battery applications (Wang *et al.*, 2011).

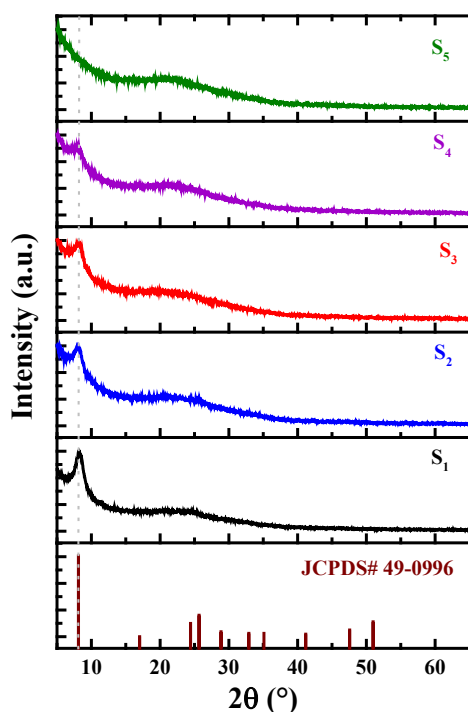


**Figure 2.** X-ray diffractions patterns of vanadium oxide with different Co<sup>2+</sup> concentrations.

**Figura 2.** Patrones de difracción de rayos X de óxido de vanadio con diferentes concentraciones de Co<sup>2+</sup>.

To complement the AFM results, SEM micrographs of S<sub>1</sub>, S<sub>3</sub> and S<sub>5</sub> samples were analyzed and are shown in Figure 4. Without cobalt addition, vanadium oxide sample S<sub>1</sub> shows a granular ground with shallow leaves. The S<sub>3</sub> sample (VO<sub>x</sub>:Cobalt salt = 50:50), presents an interconnected rings or porous arrangement, very similar to the AFM image of the

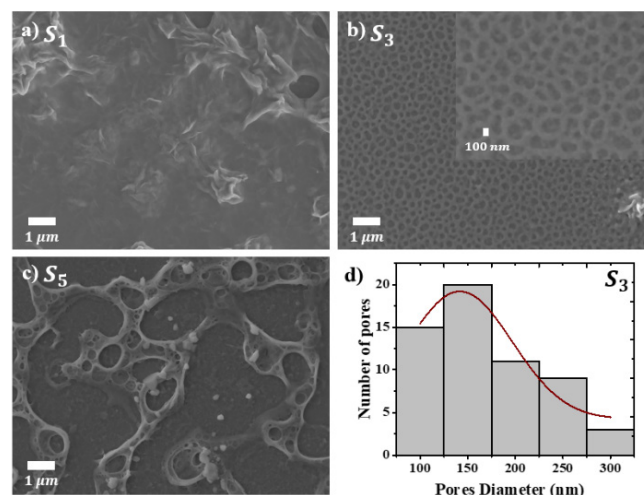


**Figure 4.** SEM micrographs with different magnifications of a) S<sub>1</sub>, b) S<sub>3</sub>, c) S<sub>5</sub> and d) histogram of S<sub>3</sub> pores.

**Figura 4.** micrografías de microscopía electrónica de barrido con diferentes magnificaciones de las muestras a) S<sub>1</sub>, b) S<sub>3</sub>, c) S<sub>5</sub> y d) histograma de los poros de la muestra S<sub>3</sub>.

same sample (Fig. 3c). The pore size distribution histogram of this film sample is in Figure 4d. It shows that the pore size varies from 100 to 300 nm, and those with ~150 nm predominates. By chemical element mapping in the SEM image of sample S<sub>3</sub>, vanadium and cobalt elements have been detected to have a homogeneous distribution inside the pores. Finally, the sample with the highest concentration of cobalt, S<sub>5</sub>, shows an irregular porous granular pattern at the surface, and under such pattern a continuous film is observed.

### Chemical composition

To assess the chemical state of the VO<sub>x</sub>:Co<sup>2+</sup> film samples, an accurate peak-fitting analysis of their X-ray photoelectron spectra (XPS) (A. Herera-Gomez, no date) was carried on.

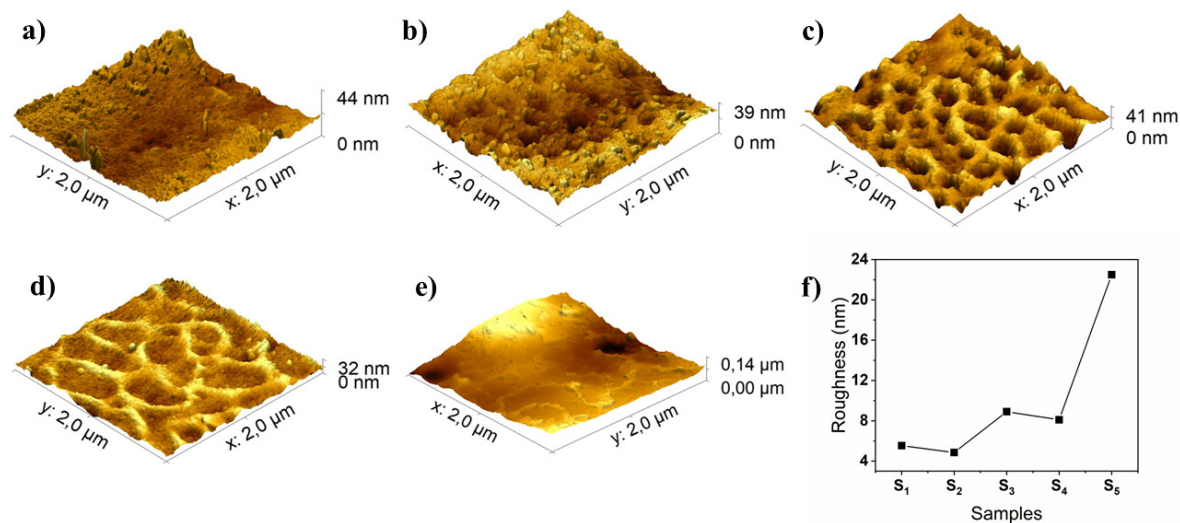


**Figure 3.** Three-dimensional AFM surface morphology images of (a) S<sub>1</sub>, (b) S<sub>2</sub>, (c) S<sub>3</sub>, (d) S<sub>4</sub>, (e) S<sub>5</sub> samples. (f) Roughness values of the same samples.

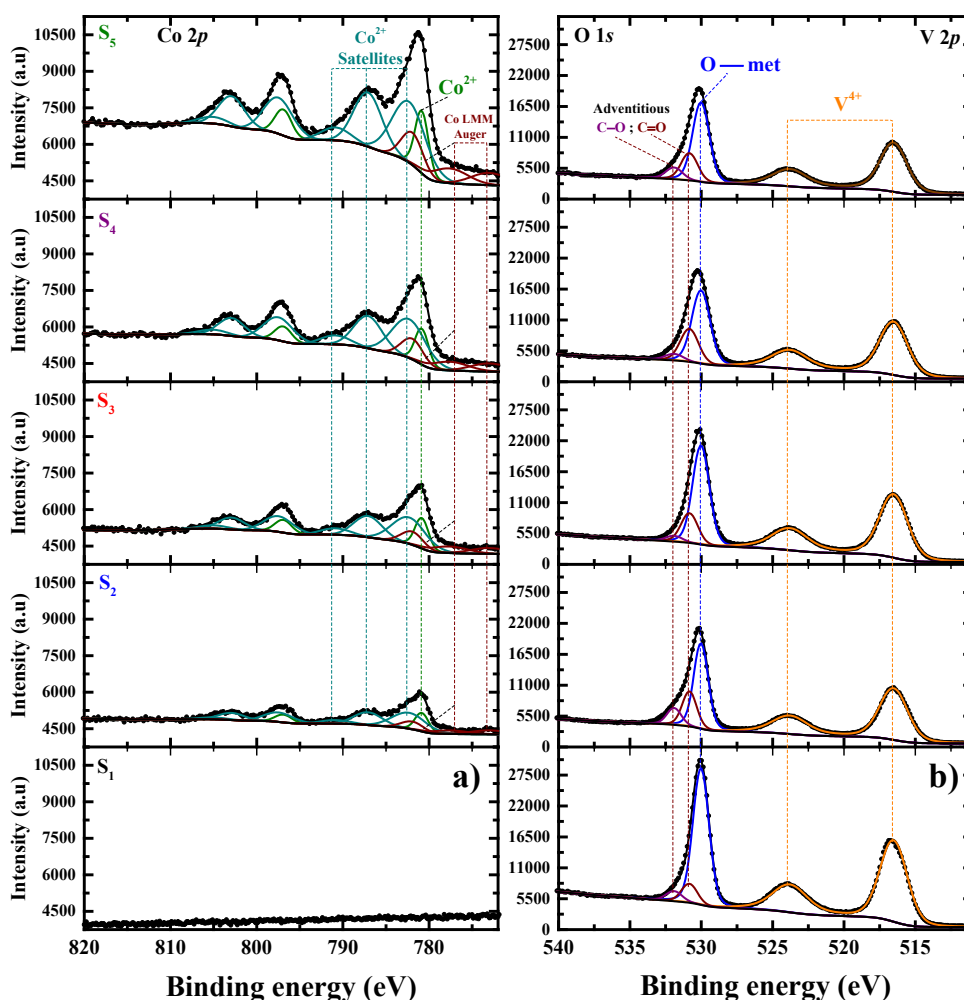
**Figura 3.** Imágenes tridimensionales por AFM de la morfología superficial de las muestras (a) S<sub>1</sub>, (b) S<sub>2</sub>, (c) S<sub>3</sub>, (d) S<sub>4</sub> y (e) S<sub>5</sub>. (f) Valores de aspereza de las mismas muestras.

Figure 5 shows the photoelectron spectra of the five samples corresponding to the (a) Co 2p and (b) O 1s and V 2p core-levels. From the Co 2p spectra (Figure 5a) we observe that the experimental data are congruent to that of the Co<sup>2+</sup> chemical state, showing the main peak centered at 780.80 eV, but at the same time, three satellite peaks at higher binding energies that are characteristics of the Co<sup>2+</sup> state (Yang *et al.*, 2010; Biesinger *et al.*, 2011; Martínez-Gil *et al.*, 2020). It is important to mention that the relative intensities of those satellite peaks suggest that there are neighboring atoms arranged in a short-range order, possibly having distortions that deviate from the octahedral Co<sup>2+</sup> symmetry. That is, the intensities of the satellite peaks are proportional to the molecular defects or amorphous state of the material, which correlates to the amorphous XRD results for all samples.

The V 2p and the O 1s spectra share the same binding energy range (Figure 5b), where we can observe the sole presence of a vanadium oxide. Due to the large spread of the reported binding energy values of this compound, to assess the present films we have employed the method proposed by Hryha *et al.* (Hryha, Rutqvist and Nyborg, 2012), where instead of using only the energy position of the V 2p<sub>3/2</sub> for che-

mic state determination, we have taken into account the difference in the binding energy between the O 1s and the V 2p<sub>3/2</sub> core levels ( $\Delta = BE(O1s) - BE(V2p_{3/2})$ ). The results show that for all samples the energy separation is around 13.50 eV, which suggests that the oxide obtained with our chemical process is VO<sub>2</sub> (Hryha, Rutqvist and Nyborg, 2012). Here it is interesting to note that the energy position of the V 2p<sub>3/2</sub> in our samples is at 516.50 eV, which is almost the average value of those reported for VO<sub>2</sub> (515.95 eV) and V<sub>2</sub>O<sub>5</sub> (517.20 eV), however, due to also the large spread in binding energy calibrations in the literature, we discard the possibility of the V<sub>2</sub>O<sub>5</sub> compound.

From peak intensities directly derived from the photoelectron spectra, chemical compositions of our VO<sub>x</sub>:Co<sup>2+</sup> film samples have been determined. We have corrected the peak intensities with the appropriate physical parameters accounting for the photoemission signal attenuation due to scattering (Cabrera-German, Gomez-Sosa and Herrera-Gomez, 2016). The results expressed in terms of atomic percentage for each of the observed chemical species are presented in Figure 6a. Here, we observe that as the Co<sup>2+</sup> concentration in the precursor solution increases, the amount of Co<sup>2+</sup> in the



**Figure 5.** X-ray photoelectron spectra of VO<sub>x</sub>:Co<sup>2+</sup> films with different concentrations of Co<sup>2+</sup>.

**Figura 5.** Espectro de rayos X de películas de VO<sub>x</sub>:Co<sup>2+</sup> con diferentes concentraciones de Co<sup>2+</sup>.

deposited films also increases, from 0 to 16.55 at %. On the other hand, the V<sup>4+</sup> atomic concentration in all five samples vary slightly, from 31 at % (sample S<sub>1</sub>) to 27 at % (sample S<sub>5</sub>), which suggests that the VO<sub>x</sub> yield is high in all the probed samples. We can also observe that the percentage of oxygen atoms bonded to metals is coherent to the chemical species: VO<sub>2</sub> and CoO, reaching 69 at % for sample S<sub>1</sub> and decreasing up to 56.4 at % for sample S<sub>5</sub> as the Co<sup>2+</sup> in the films is the largest. The atomic ratio of vanadium versus cobalt (V:Co) in each sample is listed in Table 1, changing from 6.6:1 (S<sub>2</sub>), 4.9:1 (S<sub>3</sub>), 2.9:1 (S<sub>4</sub>) to 1.6:1 (S<sub>5</sub>).

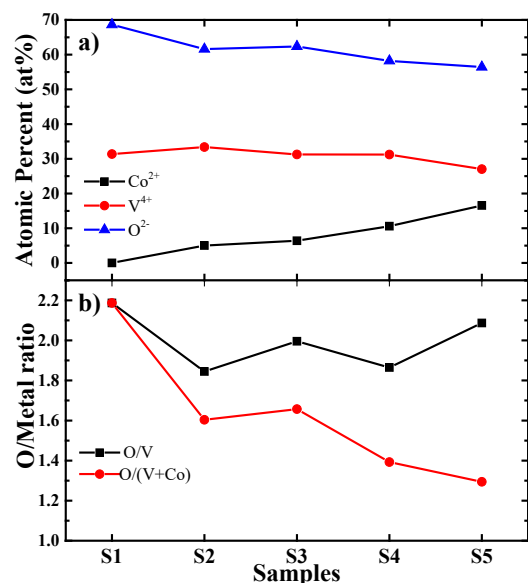


Figure 6. XPS chemical composition assessment: (a) atomic percentage (at%) of elements O, V and Co, and (b) O/V and O/(V+Co) atomic ratios of VO<sub>x</sub>:Co<sup>2+</sup> thin films.

Figura 6. Evaluación de la composición química por XPS: (a) porcentaje atómico (at%) de los elementos O, V y Co, y (b) proporciones atómicas O/V y O/(V+Co) de las películas delgadas de VO<sub>x</sub>:Co<sup>2+</sup>.

For a better assessment of metal oxide compositions in the film samples, the ratio between oxygen and metal concentrations is plotted in Figure 6b. Here, the O/V atomic ratio lies around the expected stoichiometry of VO<sub>2</sub> for all the samples, which further confirms our previous analysis. Yet, if we determine the atomic ratio of oxygen to the sum of the two metallic species, O/(V+Co), we observe that such ratio decreases with increasing concentration of Co<sup>2+</sup> in the reaction solution, a trend that follows the expected stoichiometry of the CoO compound.

## CONCLUSIONS

We demonstrate that amorphous thin films of cobalt doped vanadium dioxide can be prepared from spin-coating with a simple solution method without using any ligand or surfactant. Optical band gaps of those films are of ~2.3 eV, with higher absorption coefficients for cobalt doped samples. From detailed quantitative photoelectron analysis, we conclude that there is only one oxidation state of vanadium in all the

film samples, V<sup>4+</sup>, giving predominantly VO<sub>2</sub> products. The formation of cobalt oxide is also confirmed by XPS, showing a Co<sup>2+</sup> oxidation state corresponding to possibly disordered oxygen atoms in an octahedral, correlates to the amorphous nature of the films. Furthermore, the surface morphology of the VO<sub>2</sub>:Co<sup>2+</sup> thin films is largely influenced by the cobalt concentration, giving interconnected circle pore network when the V:Co atomic ratio is around 4.9:1. The wide band gap properties with porous surface structure make these semiconductor thin films promising for cathode material in lithium battery applications.

## ACKNOWLEDGMENTS

The authors acknowledge the technical assistance of M.L. Ramon-Garcia for XRD measurements, R. Moran-Elvira for SEM analysis, G. Casarrubias-Segura for AFM analysis, and M.R. Banda in XPS data acquisition. The project USO316007880 from División de Ingeniería at the University of Sonora is also recognize. Francisco Hernandez Guzman gratefully acknowledges PRODEP grant with the scholarship No. 511-6/2019-13924.

## REFERENCES

- A. Herera-Gomez (no date) *AAnalyzer a peak-fitting program for photoemission data*. Available at: <http://rdataa.com/aanalyzer/aanaHome.htm> (Accessed: 18 April 2020).
- Bae, J. W., Koo, B. R. and Ahn, H. J. (2019) 'Fe doping effect of vanadium oxide films for enhanced switching electrochromic performances', *Ceramics International*, 45(6), pp. 7137–7142. doi: 10.1016/j.ceramint.2018.12.219.
- Biesinger, M. C. *et al.* (2011) 'Resolving surface chemical states in XPS analysis of first row transition metals, oxides and hydroxides: Cr, Mn, Fe, Co and Ni', *Applied Surface Science*, 257(7), pp. 2717–2730. doi: 10.1016/j.apsusc.2010.10.051.
- Cabrera-German, D., Gomez-Sosa, G. and Herrera-Gomez, A. (2016) 'Accurate peak fitting and subsequent quantitative composition analysis of the spectrum of Co 2p obtained with Al K $\alpha$  radiation: I: cobalt spinel', *Surface and Interface Analysis*, 48(5), pp. 252–256. doi: 10.1002/sia.5933.
- Channu, V. S. R. *et al.* (2011) 'Electrochemical properties of polyaniline-modified sodium vanadate nanomaterials', *Applied Physics A: Materials Science and Processing*, 104(2), pp. 707–711. doi: 10.1007/s00339-011-6325-0.
- Fuentes-Ríos, J. L. *et al.* (2021) 'Modulation of the Pb/Sn ratio in Pb1-xSnxS thin films synthesized by chemical solution deposition', *Materials Science in Semiconductor Processing*, 136(July). doi: 10.1016/j.mssp.2021.106126.
- Geng, X. *et al.* (2022) 'Tuning Phase Transition and Thermochemical Properties of Vanadium Dioxide Thin Films via Cobalt Doping', *ACS Applied Materials and Interfaces*. doi: 10.1021/acsmi.2c03113.
- Hajzeri, M. *et al.* (2012) 'Sol-gel vanadium oxide thin films for a flexible electronically conductive polymeric substrate', *Solar Energy Materials and Solar Cells*, 99, pp. 62–72. doi: 10.1016/j.solmat.2011.03.041.
- Ho, H. C. *et al.* (2019) 'High quality thermochemical VO<sub>2</sub> films prepared by magnetron sputtering using V2O5 target with in situ annealing', *Applied Surface Science*, 495(July), p. 143436. doi: 10.1016/j.apsusc.2019.07.178.

- Hryha, E., Rutqvist, E. and Nyborg, L. (2012) 'Stoichiometric vanadium oxides studied by XPS', *Surface and Interface Analysis*, 44(8), pp. 1022–1025. doi: 10.1002/sia.3844.
- Hu, F. *et al.* (2017) 'Synthesis and electrochemical performance of NaV6O15 microflowers for lithium and sodium ion batteries', *RSC Advances*, 7(47), pp. 29481–29488. doi: 10.1039/c7ra04388k.
- Ji, C. *et al.* (2018) 'High thermochromic performance of Fe/Mg co-doped VO2 thin films for smart window applications', *Journal of Materials Chemistry C*, 6(24), pp. 6502–6509. doi: 10.1039/c8tc01111g.
- Khatibani, A. B., Abbasi, M. and Rozati, S. M. (2016) 'Peculiarities of deposition times on gas sensing behaviour of vanadium oxide thin films', *Acta Physica Polonica A*, 129(6), pp. 1245–1251. doi: 10.12693/APhysPolA.129.1245.
- Li, B. *et al.* (2019) 'Tungsten doped M-phase VO2 mesoporous nanocrystals with enhanced comprehensive thermochromic properties for smart windows', *Ceramics International*, 45(4), pp. 4342–4350. doi: 10.1016/j.ceramint.2018.11.109.
- Liu, S. *et al.* (2020) 'One-step microwave-controlled synthesis of CoV2O6·2H2O nanosheet for super long cycle-life battery-type supercapacitor', *Electrochimica Acta*, 364, p. 137320. doi: 10.1016/j.electacta.2020.137320.
- Lu, C. *et al.* (2019) 'Terahertz Transmittance of Cobalt-Doped VO2 Thin Film: Investigated by Terahertz Spectroscopy and Effective Medium Theory', *IEEE Transactions on Terahertz Science and Technology*, 9(2), pp. 177–185. doi: 10.1109/THZ.2019.2894516.
- Mane, A. A. and Moholkar, A. V. (2017) 'Effect of film thickness on NO2 gas sensing properties of sprayed orthorhombic nanocrystalline V2O5 thin films', *Applied Surface Science*, 416(2), pp. 511–520. doi: 10.1016/j.apsusc.2017.04.097.
- Martinez-Gil, M. *et al.* (2020) 'Effect of annealing temperature on the thermal transformation to cobalt oxide of thin films obtained via chemical solution deposition', *Materials Science in Semiconductor Processing*, 107(October 2019). doi: 10.1016/j.mssp.2019.104825.
- Peng, B. *et al.* (2018) 'Transparent AlON ceramic combined with VO2 thin film for infrared and terahertz smart window', *Ceramics International*, 44(12), pp. 13674–13680. doi: 10.1016/j.ceramint.2018.04.205.
- Petnikota, S. *et al.* (2018) 'Amorphous Vanadium Oxide Thin Films as Stable Performing Cathodes of Lithium and Sodium-Ion Batteries', *Nanoscale Research Letters*, 13, pp. 1–13. doi: 10.1186/s11671-018-2766-0.
- Sharma, G. P. *et al.* (2021) 'Chalcogenide Dopant-Induced Lattice Expansion in Cobalt Vanadium Oxide Nanosheets for Enhanced Supercapacitor Performance', *ACS Applied Energy Materials*, 4(5), pp. 4758–4771. doi: 10.1021/acsaem.1c00357.
- Shen, N. *et al.* (2021) 'Vanadium dioxide for thermochromic smart windows in ambient conditions', *Materials Today Energy*, 21, p. 100827. doi: 10.1016/j.mtener.2021.100827.
- Silversmit, G. *et al.* (2004) 'Determination of the V2p XPS binding energies for different vanadium oxidation states (V5+ to V0+)', *Journal of Electron Spectroscopy and Related Phenomena*, 135(2–3), pp. 167–175. doi: 10.1016/j.elspec.2004.03.004.
- Silversmit, G. *et al.* (2006) 'An XPS study on the surface reduction of V2O5(0 0 1) induced by Ar+ ion bombardment', *Surface Science*, 600(17), pp. 3512–3517. doi: 10.1016/j.susc.2006.07.006.
- Tabatabai Yazdi, S., Pilevar Shahri, R. and Shafei, S. (2021) 'First synthesis of In-doped vanadium pentoxide thin films and their structural, optical and electrical characterization', *Materials Science and Engineering B: Solid-State Materials for Advanced Technology*, 263(August 2020), p. 114755. doi: 10.1016/j.mseb.2020.114755.
- Wang, S. *et al.* (2011) 'Three-dimensional porous V2O5 cathode with ultra high rate capability', *Energy and Environmental Science*, 4(8), pp. 2854–2857. doi: 10.1039/c1ee01172c.
- Wang, S. *et al.* (2020) 'Facile synthesis of VO2 (D) and its transformation to VO2(M) with enhanced thermochromic properties for smart windows', *Ceramics International*, 46(10), pp. 14739–14746. doi: 10.1016/j.ceramint.2020.02.278.
- Xu, Y. *et al.* (2019) 'Ammonium Vanadium Bronze as a Potassium-Ion Battery Cathode with High Rate Capability and Cyclability', *Small Methods*, 3(8), pp. 1–9. doi: 10.1002/smt.201800349.
- Yang, J. *et al.* (2010) 'Synthesis and characterization of Cobalt hydroxide, cobalt oxyhydroxide, and cobalt oxide nanodiscs', *Journal of Physical Chemistry C*, 114(1), pp. 111–119. doi: 10.1021/jp908548f.
- Yao, X. *et al.* (2018) 'Cesium-Doped Vanadium Oxide as the Hole Extraction Layer for Efficient Perovskite Solar Cells', *ACS Omega*, 3(1), pp. 1117–1125. doi: 10.1021/acsomega.7b01944.
- Yuan, L. *et al.* (2021) 'In-Situ thermochromic mechanism of Spin-Coated VO2 film', *Applied Surface Science*, 564(June), p. 150441. doi: 10.1016/j.apsusc.2021.150441.
- Zhan, Y. *et al.* (2020) 'Tuning thermochromic performance of VOx-based multilayer films by controlling annealing pressure', *Ceramics International*, 46(2), pp. 2079–2085. doi: 10.1016/j.ceramint.2019.09.188.
- Zhou, X. *et al.* (2020) 'Abnormal dependence of microstructures and electrical properties of Y-doped VO2 thin films on deposition temperature', *Ceramics International*, 46(11), pp. 18315–18321. doi: 10.1016/j.ceramint.2020.05.053.